Dual Bioresponsive Mesoporous Silica Nanocarrier as an "AND" Logic Gate for Targeted Drug Delivery Cancer Cells

*Xin Chen, Alexander H. Soeriyadi, Xun Lu, Sharon M. Sagnella, Maria Kavallaris, and J. Justin Gooding**

Despite the rapid development of drug delivery vehicles that react to a specific biological environment, the complexity of triggering drug release in a particular target area remains an enduring challenge. Here, the engineering of bioresponsive polymer-mesoporous silica nanoparticles (MSNs) with function akin to an AND logic gate is described. Polycaprolactone (esterase degradable) is immobilized into the core of MSNs while polyacrylic acid (PAA), which is pH responsive, covered the outside of the MSNs to create a PAA-PCL-MSNs construct. Fluorescence spectroscopy indicates that the construct releases the payload (doxorubicin, cancer drugs) in the presence of, and only in the presence of, both low pH AND esterase. Confocal microscopy and fluorescence lifetime microscopy (FLIM) demonstrate uptake of the intact construct and subsequent intracellular doxorubicin (DOX) delivery into the nucleus. Further in vitro IC_{50} studies demonstrate the AND logic gate delivery system results in more than an eightfold efficacy against neuroblastoma (SK-N-BE(2)) cells in comparison with normal fibroblasts (MRC-5). These results demonstrate the utility of MSN-polymer construct to create an AND gate capable of selectively delivering a drug payload.

1. Introduction

The realization of a "magic bullet", a term coined by Paul Ehrlich in relation to therapy, has been a significant scientific challenge of our time.[1] Over the past decades, intelligent materials that can communicate and respond to their environment have been exploited as drug delivery vehicles.[2] Nanoscale carriers capable of drug release under certain physiological conditions such as changes in pH,[3] temperature,[4] reactive oxygen species (ROS)[5] and enzymes[6] have been developed.[2b,7] Changes in pH and enzymatic triggers are of particular interest in the development of controlled drug delivery systems as anti-cancer therapies due to their endogenous existence in tumour environments.[8] Previous studies have demonstrated that the pH of extracellular fluid in tumour tissue is about 6.5 with a range of 5.7–7.0,[8a] which is lower than the pH of normal tissue (pH 7.4).[9] Another physical characteristic of tumours that can be exploited is the enhanced permeation and retention effect (EPR) whereby nanoparticles preferentially deposit at the tumour site via passive targeting.[10] Examples of drug delivery vehicles that have been employed as therapeutic delivery vehicles are liposome, polymeric micelles, dendrimers, nanoparticle and polymersome.[11]

One material that has emerged as a promising candidate and exhibits many of the desirable characteristics described above is mesoporous silica nanoparticle (MSN). MSNs possess a number of advantages including biocompatibility, high drug loading capacity, biodegradability, zero premature release and ease of functionalization.[12] For this reason, there have been many responsive MSN drug delivery system developed such as pH,[13] light,[14] magnet,[15] ROS,[16] and enzyme.[17] Dual responsive MSNs with combination such as temperature-light,[18] pH-redox,[12a,19] pH-temperature,[20] or pH-ATP[21] have also been employed. All of these dual responsive materials have utilized an "OR" logic gate which lead to drug release in the presence of either stimuli in the system. Notable exception is work by Angelos et al. which was the first to report an "AND" logic gate MSN system that was responsive to visible light and elevated pH.[22] However, the application of the "AND" logic gate has not been explored yet as well as the stimuli is not the best option for drug delivery application as it requires external triggers. In recent work, Xiao et al.[12a] has demonstrated a dual pH and redox stimuli responsive MSN system to deliver anti-cancer drugs. However, in that work, drug release also occurs in the presence of only reducing agent, such as glutathione in human blood, regardless of the pH, albeit at smaller rate as reducing agent. Hence, in fact only one stimulus is required. Drawing inspiration from previous work, we aim to design a drug delivery vehicle with a true "AND" logic gate where drug release can only happen if two stimuli are delivered. Furthermore, in our case both these stimuli arise from the biochemistry of the pathology, such that the drug is released only where required and when required.

Dr. X. Chen, Dr. A. H. Soeriyadi, X. Lu, Prof. J. J. Gooding
School of Chemistry and Australian Centre for NanoMedicine
University of New South Wales
Sydney, 2052, Australia
E-mail: justin.gooding@unsw.edu.au
Dr. S. M. Sagnella, Prof. M. Kavallaris
Children's Cancer Institute Australia for Medical Research
Lowy Cancer Research Centre and Australian Centre for NanoMedicine
University of New South Wales
Sydney, 2052, Australia

DOI: 10.1002/adfm.201402339

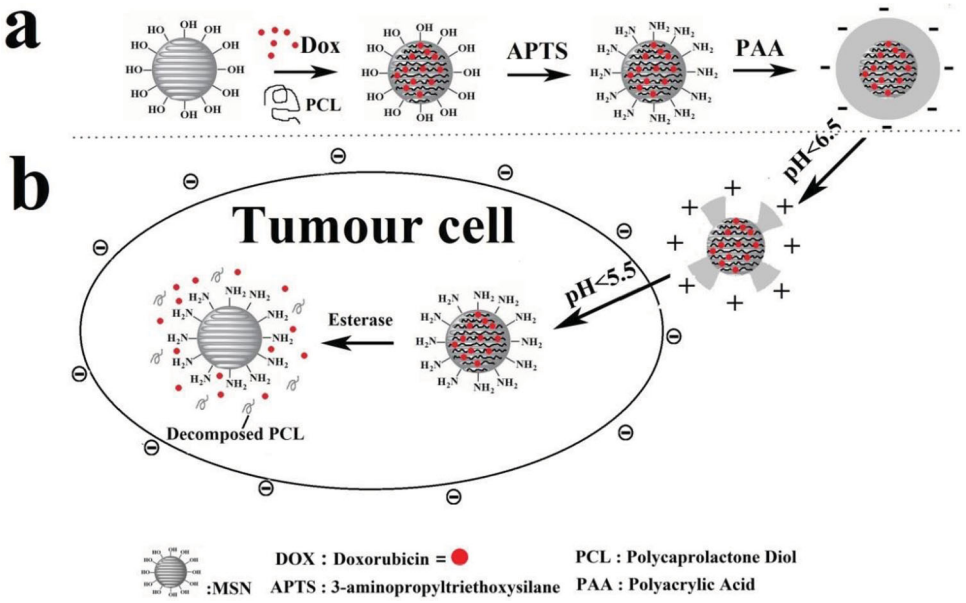

Scheme 1. a) Formation of PAA and PCL multiple functionalized MSN (PAA-PCL-MSNs). b) Schematic representation of PAA-PCL-MSNs based selective drug delivery system. The selectivity is achieved by pH triggered removal of PAA (pH < 6.5) and enzyme (esterase) triggered decomposition of PCL.

Such a strategy will lead to a more specific payloads transfer.[23] The requirement of accurate targeting is especially needed for cancer treatment because of the high toxicity of many anticancer drugs to normal cells and cancer cells. Thus, the design of delivery vehicles with an "AND" gate with physiological stimuli (pH and enzyme) would be of considerable advance towards the development of "magic bullet" therapies. As has been well documented and experience, current standard chemotherapy procedure has various side effects that is truly damaging the life quality of its patient. For example, the side effect of doxorubicin includes decrease in blood cell counts, hair loss, nausea and vomiting, and heart damage. A reduction in this side-effects is a highly desirable property of any drug delivery vehicle and we believe that the "AND" logic gate is a step forward to achieve this goal. The stepwise logic AND gate provided by the PAA-PCL-MSNs designed in this work, avoids premature or unexpected release of the cargo before cell internalization that could occur with pH only responsive systems, or in an enzyme only response system.[17a,24]

Herein, we report a versatile and effective strategy for the preparation of pH "AND" enzyme logic gate polymer-functionalized MSNs that are able to display selective and controlled cargo delivery in tumour cells (**Scheme 1**). In this work, control of the MSN pores gates was achieved by filling the pores with polycaprolactone (PCL) and the covering the outer surface with polyacrylic acid (PAA). Both polymers have been reported as biocompatible materials with potential applications as components of drug delivery vehicles.[25] In its closed condition, the PAA-PCL-MSN construct bears a negative surface charge with its cargo stored within the pores. At a pH of 5.5 found around tumour cells,[9,26] the PAA shell will disassociate from the surface of the MSN construct due to cleavage of the hydrogen bond, resulting in a positively charged construct (Scheme 1). The positively charged MSN construct then undergoes endocytosis via the negatively charged cell membrane.[10,12e] The release of the cargo only occurs upon cleavage of the PAA (at low pH) AND digestion of the PCL (in the presence of esterase) in a stepwise manner.

2. Result and Discussion

2.1. Synthesis and Characterization of PAA-PCL-MSNs

The mesoporous structure was templated by cetyltrimethylammonium bromide (CTAB) surfactants, and further extended to a larger size (>20 nm) by 1,3,5-trimethylbenzene (pore-expanding agent).[27] For the preparation of the PAA-PCL-MSN construct, the as-synthesized MSNs were first loaded with Rhodamine 6G (model drug) and/or doxorubicin (anti-cancer drug), meanwhile the polycaprolactone diol was inserted into the pores through hydrophobic interactions. Next, the MSN-PCL construct was reacted with 3-aminopropyltriethoxysilane to introduce the amino groups on the internal and external surfaces of the MSNs. The internal amino groups were used to form hydrogen bonds with PCL and further restrict the drugs in the pores, and the external amino groups form H-bonds with PAA. Transmission electron microscopy (TEM) showed 200 nm spherical MSN (Figure S1a, Supporting Information) with similar size after immobilization of the polymers (Supporting Information, Figure S1b,c). N_2 adsorption–desorption isotherm experiments with Brunauer-Emmett-Teller (BET) calculation indicated the complete blockage of the PAA-PCL-MSNs as can be seen from **Figure 1** and **Table 1**(from ± 25 nm to < 1 nm). Furthermore, the sequential polymer immobilization steps were investigated by infrared (IR) spectra and nuclear magnetic resonance (NMR) (Figure S2–S5, Supporting Information) which reveal successful modification of the MSNs with both PCL and PAA. The drug loading percentage was determined using ultraviolet-visible (UV-vis) spectra at 500 nm (for DOX)

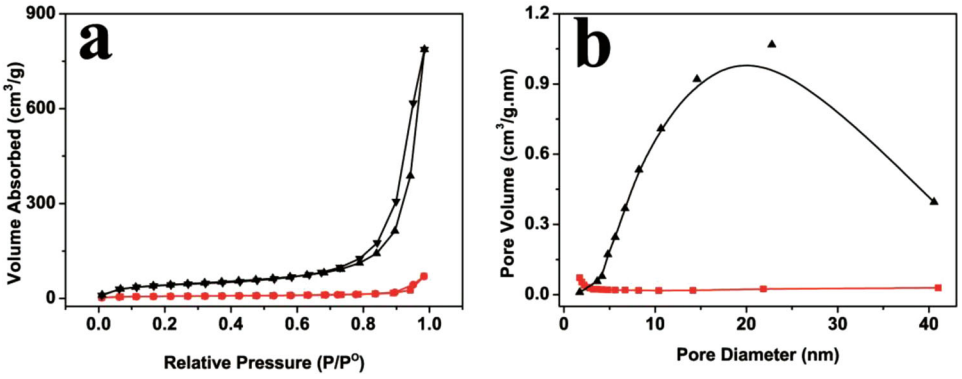

Figure 1. a) N_2 adsorption desorption isotherms and b) pore-size distribution of bare MSNs (black curve) and after immobilization of polymers PAA-PCL-MSNs after Rhodamine 6G loading (red curve). The adsorption-desorption isotherm showing significant reduction of the pore volume and diameter to virtually 0 nm after polymer covering.

and 550 nm (for Rhodamine 6G). The drug loading percentage was up to 0.3 gram per gram of PAA-PCL-MSNs (Figure S6, Supporting Information). Unlike other MSNs modification procedures reported previously, in this work the exterior surface of the MSN and the pore space are modified with two different polymers.[12b] One can envisage that this highly versatile design could be implemented with various other responsive polymers.

2.1.1. Logic "AND" Gate Controlled Release

The controlled release profile of payload (Rhodamine 6G or DOX) from polymer-functionalized MSNs was investigated under simulated physiological conditions (i.e., pH range 5.5-7.4 AND the presence or absence of esterase). The amount of payload released from MSNs was determined by monitoring the emission of the payload in the solution as a function of time. It can be seen from **Figure 2** and Figure S7 (Supporting Information) that both pH AND esterase are necessary to trigger the drug release from PAA-PCL-MSNs. Quantification of the final release percentages of DOX from PAA-PCL-MSNs after 50 h incubation at low pH only is <5% as well as there is no significant leakage of dye when the stimuli presence is only presence of enzyme (Figure **2**). There is a slight leakage of Rhodamine G at lower pH (PAA removal from the MSN exterior) (Figure S7, Supporting Information). This is could be because there is a slight amount of physical absorption of payloads to the surface of the MSNs system. In contrast, at acidic condition (pH = 5.5) AND in the presence of esterase, the release of the payload dramatically increased over time, with the cumulative release of payload reaching ≈90% over 50 h. This data demonstrate the powerful and versatile technique to create an AND gate through modification of the outer and inner pores of MSNs.

The design here also takes account of the environment of tumours where low pH and high esterase concentration occur within the cells. Thus a slight payloads leakage is deemed acceptable as the payloads will be in cancer cells environment. The ability of preventing premature release is of importance and the "AND" logic provide better gate in comparison to single stimuli system. For example, in recent work it was shown that a PAA covered MSN has the ability to control drug release although it could leads up to 30% of payload release in its "closed" state over 24 h period.[24] In another system, an esterase responsive MSN system, payload release was observed at around 10% over 10 h period.[17a] Thus, the "AND" demonstrated that the dual polymeric system could be a solution in minimizing the payload premature release.

Table 1. The structure parameters of bare MSNs and PAA-PCL-MSNs loaded with Rhodamine 6G.

Samples	BET surface area [m^2/g]	Pore volume [mL/g]	Peak pore diameter [nm]
MSNs	402.85	0.96	22.83
PAA-PCL-MSNs loaded with Rhodamine 6G	38.63	0.05	< 1

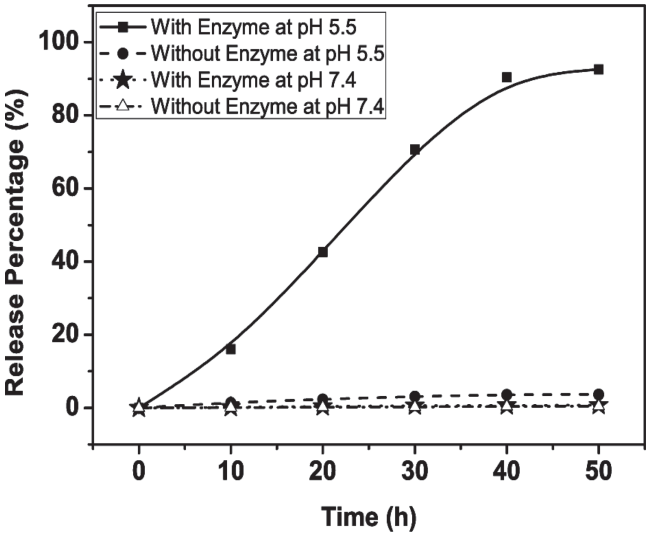

Figure 2. pH and esterase multiple-dependent release kinetics of doxorubicin (DOX) loaded PAA-PCL-MSNs. The figure is represented by ■ (pH 5.5 in present of 4 mg/L esterase), ● (pH 5.5 in absent of esterase), ★ (pH 7.4 in present of 4 mg/L esterase), and Δ (pH 7.4 in absent of esterase). The release percentage is calculated by or UV–Vis absorption measurement.

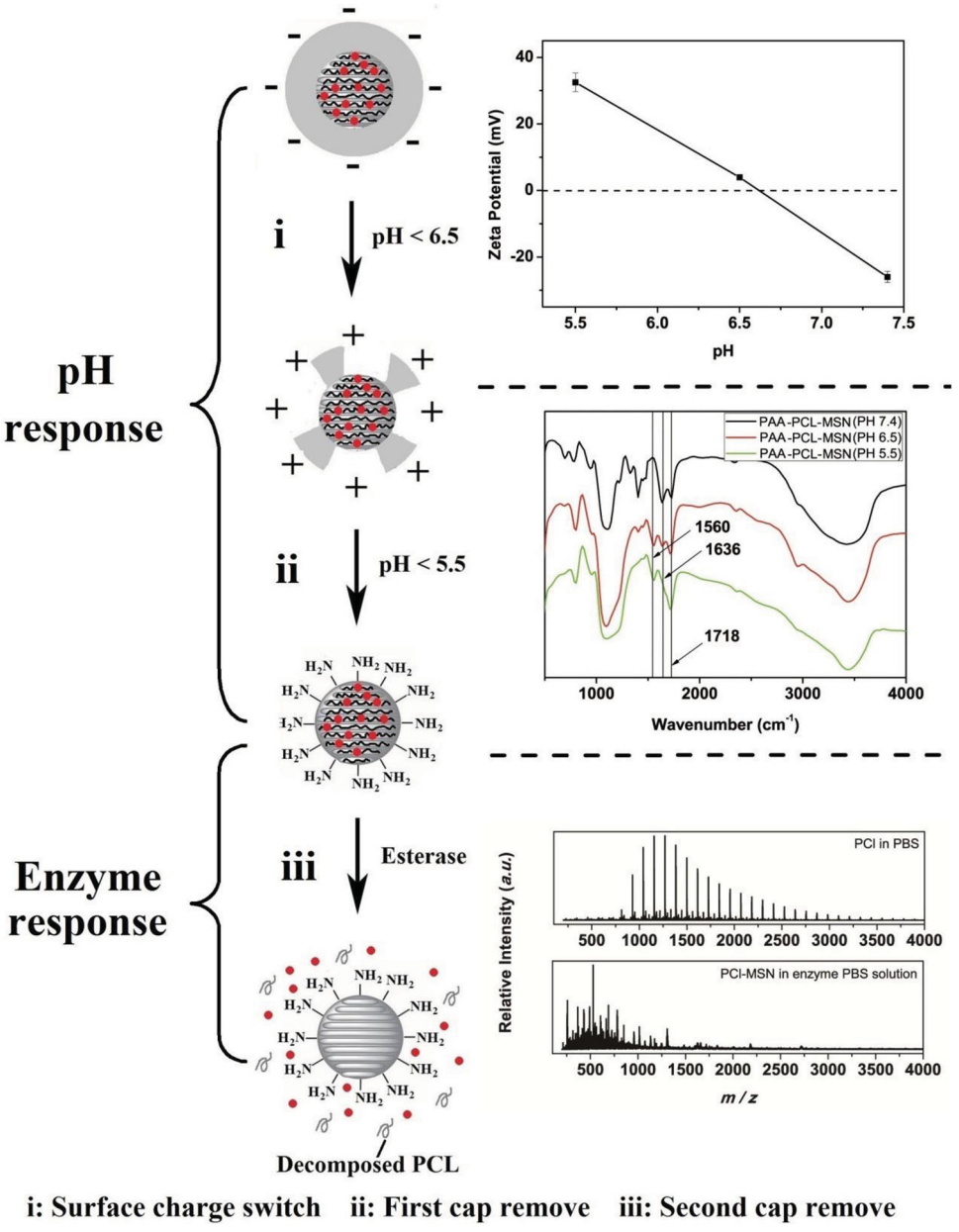

Figure 3. i) pH-responsive surface charge change presented by schematic representation and pH-dependent zeta potential of PAA-PCL-MSNs. ii) pH-responsive cap opening and the interaction followed by IR. iii) Enzyme-responsive cap two opening and mass spectra of PCL-MSNs after incubation in PBS buffer with and without esterase.

To further understand the mechanism of the drug release, several analytical and characterization were performed. Thermogravimetric analysis (TGA, Figure S9) provided further information on the composition of the PAA-PCL-MSNs construct. The TGA analysis indicated the MSNs were modified with around 17 wt% of both PAA and PCL. TGA also showed the degradation of the different polymers upon exposure to the different stimuli. As can be seen from Figure S9 (Supporting Information), there is 17% removal of the PAA after 24 hour incubation in pH 5.5 solution. A further 12% polymer loss was observed with the addition of esterase in the low pH solution. These results indicate all of PAA were effectively removed and more than 70% of PCL were removed from the PAA-PCL-MSNs under appropriate condition. Detail analysis of the pH and esterase response was also revealed by IR and MS spectra, respectively (**Figure 3**). As the pH decreased below the isoelectric point of 6.5, PAA starts to be cleaved from the MSN (Figure 3a). As can be seen from the IR spectra of PAA-PCL-MSNs (Figure 3b), at neutral pH, there is a strong C=O stretch peak at 1636 cm^{-1} representing the hydrogen bond between the amino and carboxyl moieties; hence showing the binding force of MSNs with the PAA cap occurs through hydrogen bonding (C=O–H–N). When the system becomes increasingly acidic, the intensity of the peak at 1718 cm^{-1} (C=O stretch

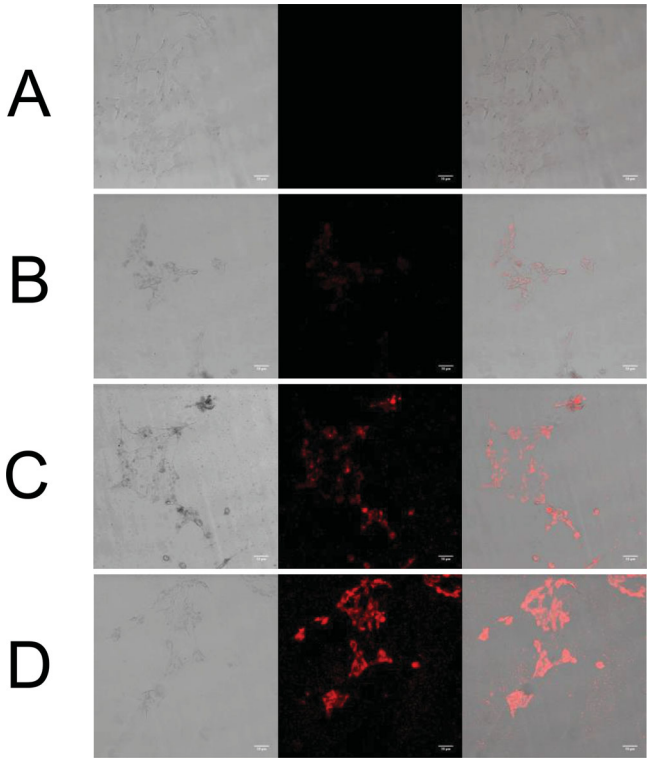

Figure 4. Optical microscope images (left), fluorescent images (middle) and overlay images (right) of SK-N-BE(2) cells a) before and after incubation with Rhodamine 6G loaded PAA-PCL-MSNs for b) 2 h, c) 4 h, and d) 24 h.

of carboxyl dimers) and 1560 cm^{-1} (N–H bending vibration) increases gradually, accompanied by the decrease of the peak at 1636 cm^{-1}. At pH = 5.5, there is a complete disappearance of the peak at 1636 cm^{-1} as well as the appearance of a peak at 1718 cm^{-1} and 1560 cm^{-1}. The IR results indicated that the protonated carboxyl tend to form dimers with strong intramolecular hydrogen bond (21 kJ/mol) instead of forming hydrogen bond with amino group on the MSN exterior which has weaker bond (8 kJ/mol), leading to the cleavage of PAA. The esterase response and removal of PCL was monitored by MS spectrometry (Figure 3c). As expected, PCL is stable in PBS (pH 7.4) in the absence of esterase. On the other hand, after 24 h incubation in the presence of 4 mg/L esterase, the mass spectrum of the PCL-functionalized MSNs shows low molecular weight fragments, indicating digestion of PCL.

2.1.2. Cellular Uptake and Release Study

The in vitro delivery and cargo release from PAA-PCL-MSNs was investigated in SK-N-BE(2) neuroblastoma cells and HeLa cervical cancer cells (**Figure 4** and Supporting Information Figure S10). PAA-PCL-MSNs loaded with Rhodamine 6G showed a time dependent uptake in SK-N-BE(2) cells, as seen in Figure 4. Prior to the addition of MSNs (Figure 4a), no fluorescent signal was detected. At 2 h post incubation with Rhodamine 6G loaded PAA-PCL-MSNs (Figure 4b), uptake is apparent as demonstrated by a weak fluorescence which appears to be localized in the cytoplasm. An increase in the incubation period to 4 h and 24 h (Figure 4c,d), resulted in a further increase in the intracellular fluorescence intensity in the SK-N-BE(2) cells. A similar uptake pattern was demonstrated for Rhodamine 6G loaded PAA-PCL-MSNs in HeLa cells (Figure S10, Supporting Information).

To examine the ability of the PAA-PCL-MSNs to effectively deliver chemotherapeutics into tumour cells, PAA-PCL-MSNs were loaded with DOX and the uptake and delivery of DOX in SK-N-BE(2) neuroblastoma cells was investigated via confocal microscopy (**Figure 5**A). Little to no free DOX is visible in the cells at 1 h, however by 4 h free DOX can be seen localized to the nucleus as is expected due DOX's mechanism of action as a DNA intercalating agent.[28] The DOX loaded PAA-PCL-MSNs show a similar localization pattern as the free DOX with two notable differences. First is the fact that DOX loaded PAA-PCL-MSNs can be detected, albeit weakly, at 1 h post incubation. Second, at 4 h post incubation, while localization of DOX in the nucleus has begun to occur, PAA-PCL-MSNs DOX also appear in the cytoplasm likely in endosomal/lysosomal compartments as a result of the difference in uptake mechanism of the nanoparticles (endocytosis) as compared to the free DOX (diffusion). As particle associated DOX cannot enter the nucleus due to size, it is expected that PAA-PCL-MSNs-DOX would be present in the cytoplasm until drug release occurs at which time DOX can then translocate into the nucleus via diffusion through the nuclear membrane.[29]

To verify that the DOX was released from the MSNs intracellularly, fluorescence lifetime imaging microscopy (FLIM) was employed. FLIM has been previously used in nanoparticle delivery of DOX to differentiate particle associated DOX from free DOX in its form.[30] This photochemical property of a fluorophore (DOX in this case) is highly dependent on its physicochemical environment, and as such, is sensitive to factors including, but not limited to, pH changes, protein binding, and polymer/nanocarrier interactions.[31] Hence, particle associated DOX consistently exhibits an increased lifetime over its free form making FLIM ideal for monitoring in vitro drug release from nanocarrier formulations. As can be seen from Figure 5B,C in which phasor plot analysis is employed, there is a distribution of the three different DOX lifetimes present in the SK-N-BE(2) cells following a 4 hr incubation with DOX-MSNs. These lifetimes appear on the phasor plot from shortest (red) to longest (turquoise) (Figure 5C). Examination of the sub-cellular distribution of these different lifetimes (Figure 5B) indicates that the three different lifetimes correspond to the following distribution: i) free DOX (red), ii) intracellular DOX-MSNs (green), and iii) DOX-MSNs in solution (turquoise). DOX loaded PAA-PCL-MSNs which have not been taken up by the cells (turquoise) exhibit the longest lifetime as the construct remains fully intact prior to cellular uptake. As discussed previously, a decrease in pH would result in the degradation and break down of the PAA from the MSN surface. Upon endocytosis, the MSNs would reside in the low pH environment of the endosomal compartment and as such, both the change in pH and PAA degradation which could occur prior to and during uptake would both affect the DOX lifetime. Thus, DOX-MSNs which have been taken up by the cells and reside in the cytoplasm of cells result in a second lifetime (green). Most

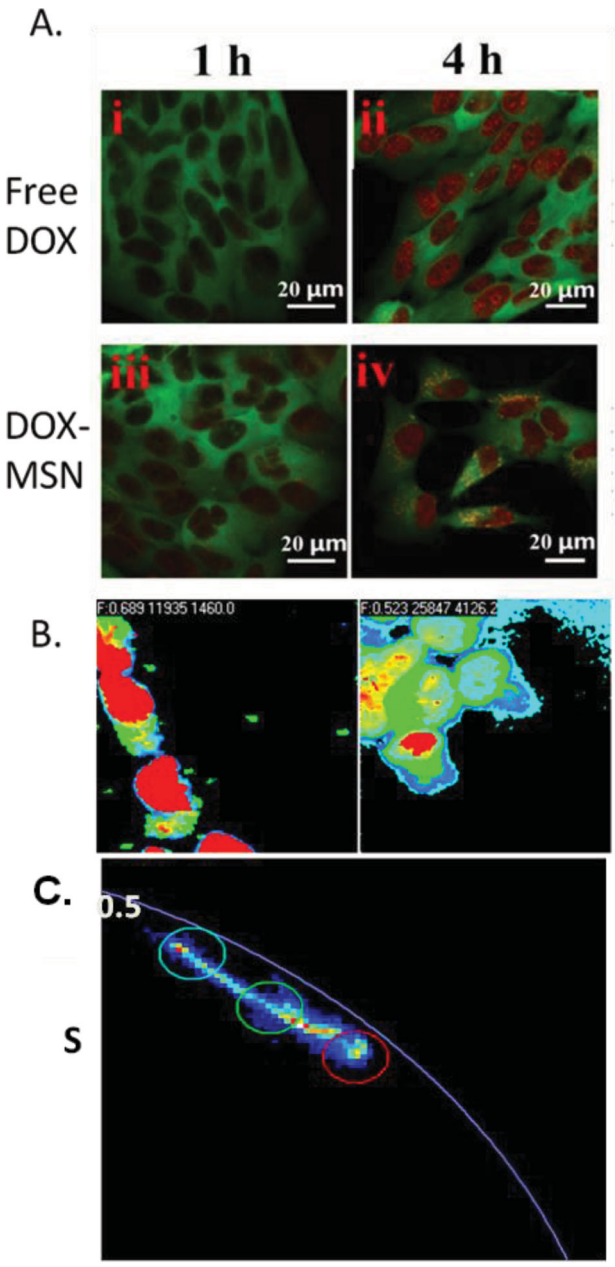

Figure 5. A) Confocal fluorescent microscope images of SK-N-BE (2) cells after incubation with free DOX (i, ii) and DOX loaded PAA-PCL-MSNs (iii, iv) for 1 h (i, iii) and 4 h (ii, iv). B,C) Fluorescence lifetime microscopy (FLIM) of DOX Loaded PAA-PCL-MSNs at 4 h. Three lifetimes are apparent corresponding to DOX-MSNs in solution or present on the outer cell membrane which have not been taken up by the cells (turquoise), DOX-MSNs which has been internalized and resides in the cytoplasm of the cell (green), and free DOX which has been released from the MSNs and is localized to the nucleus (red). B) Subcellular localization of the three different lifetimes. C) Phasor plot analysis demonstrating a change in lifetime with uptake and release of DOX-MSNs.

importantly, free DOX must be fully released from the MSN prior to nuclear localization, and only DOX with the shortest lifetime (red), known to correspond to free DOX,[30,32] is visible in the nucleus (Figure 5B). These results indicate that DOX

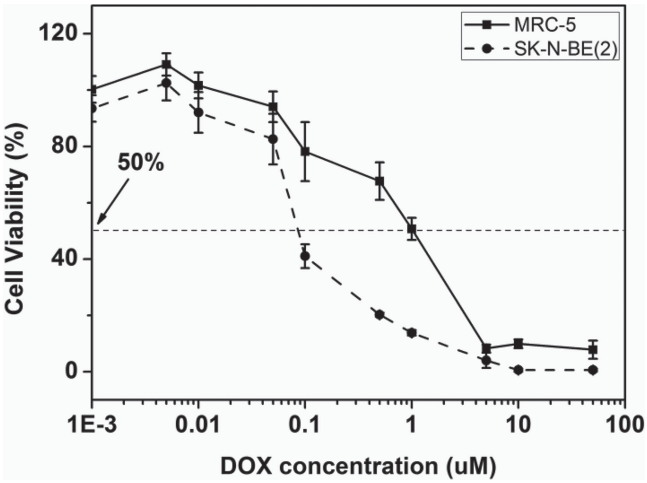

Figure 6. Viability of tumour cells (SK-N-BE (2), neuroblastoma cell) and normal cells (MRC-5, human fetal lung fibroblast cell) incubated with the increasing amounts of DOX in the form of DOX loaded PAA-PCL-MSNs.

loaded PAA-PCL-MSNs are effectively taken up across the cell membrane intact, with pH and esterase triggered release occurring intracellularly. Thus, further highlight the importance of having an "AND" logic gate to ensure the release of drug at desired target.

2.2. Cytotoxicity Study

In vitro cytotoxicity of MSNs, PCL, PAA, and PAA-PCL-MSNs construct were tested on HeLa cells using the MTT assay. As shown in Figure S11, The PAA-PCL-MSN construct and its individual components showed no obvious cytotoxic effects on the HeLa cells at 6.25–100 µg mL^{-1} after 48 h incubation. These results demonstrate that the PAA-PCL-MSNs are well-tolerated even at high concentrations, which is in good agreement with previous works on MSN, with similar results seen in both SK-N-BE(2) and MRC-5 fibroblast cells which as a normal cell type as used as a comparison to cancer cells (Figure S12, Supporting Information).[33] In vitro efficacy of DOX loaded PAA-PCL-MSNs was examined in SK-N-BE(2) and normal MRC-5 fibroblasts (**Figure 6**) via the Alamar Blue cell viability assay following 72 h incubation. As expected, the DOX loaded PAA-PCL-MSNs showed increasing toxicity to both normal and tumour cells with increasing effective DOX concentration. Through regression analysis, an IC_{50}, the half-maximal (50%) inhibitory concentration, can be calculated. The IC_{50} of the MSN-DOX was ±0.1 µM in SK-N-BE (2), and ±0.8 µM in MRC-5. This eightfold difference indicates that the DOX loaded PAA-PCL-MSNs exhibit a higher efficacy towards tumour cells than normal cells. In vitro examination of free DOX in both cell types (Figure S13, Supporting Information) demonstrated less selectivity between these two cell types.

This selectivity towards cancer cell is a highly desirable attributes of a drug delivery vehicle. Successful implementation of such drug delivery vehicle could reduce the side effects of many cancer therapeutic agent and leads to not only higher efficacy but also better life quality of patients that is undergoing

therapeutic treatment for cancer. Due to the versatility of the technique described here. One could easily envisage other cancer therapeutic drug to be incorporated into the system.

3. Conclusion

In summary, we have developed an efficient and effective strategy for the preparation of a new class of "AND" logic gate polymer-functionalized mesoporous silica nanoparticles for drug release to cancer cells. This AND logic gate MSN contains two different polymers that would open the gate in the presence of low pH followed by an enzymatic stimuli as found in tumours. The innovative way of modifying both the inside and outside of the MSNs is proven to be effective way to create an "AND" logic gate. The controllable drug release in tumour cells is based on the pH-induced cleavage of hydrogen bonds, pH-induced surface charge switching, and enzyme-mediated hydrolysis of ester bonds thereby exploiting environmental differences tumours and normal tissues. The stimuli responsive nature of these polymer-functionalized MSNs is designed to take advantage of the unique physiological environment at the site of solid tumours, making it an excellent nanocarrier candidate for therapeutic applications.

4. Experimental Section

Materials: Rhodamine 6G, doxorubicin (DOX), polycaprolactone diol (PCL, M_w = 2kDa), polyacrylic acid (PAA, M_w = 45 kDa), lipase (from *Pseudomonas cepacia*), 3-aminopropyltriethoxysilane (APTS), tetraethyl orthosilicate (TEOS), *N*-cetyltrimethylammonium bromide (CTAB), ammonium hydroxide and 1,3,5-trimethylbenzene (TMB) were purchased from Sigma-Aldrich (Sydney, Australia). All the chemicals were analytical grade and used without further treatment.

Synthesis of Mesoporous Silica Nanoparticles (MSNs): MSNs were prepared by the classical CTAB-templated, base-catalyzed sol-gel method.[27,34] The pH value of 1000 mL deionized water was adjusted to approximately 11 with 52.8 mL ammonium hydroxide (29 wt% NH_3 in water). The temperature was raised to 323 K, and then 1.12 g CTAB and subsequent 5.8 mL TEOS were added with rapid stirring. After 2 h, the mixture was aged overnight, then centrifuged and washed thoroughly with distilled water and ethanol. As-synthesized silica nanoparticles were dispersed in ethanol by sonication for 30 min, followed by the addition of 20 mL of 1:1 mixture (v/v) of water and TMB. The mixture was placed in the autoclave, and kept at 140 °C for 4 days without stirring. The resulting white powder was washed with ethanol and water five times each. The surfactant templates were then removed by extraction using acidic methanol (9 mL of HCl/400 mL of methanol, 36 h) at 70 °C, which were further centrifuged, washed several times with ethanol and dried under vacuum for 20 h.

Drug Loading and Polymer Functionalization of MSN (PAA-PCL-MSN): Typical polymer functionalization of MSN is as follows: 1 g MSN and 0.5 g Rhodamine 6G or doxorubicin was dispersed in 50 mL tetrahydrofuran, and then 300 mg PCL was added. The mixture was stirred at room temperature for 24 h. After that, the suspension was dry at 40 °C in the oven over night to remove the tetrahydrofuran. Then the resulting powder was moved into a Schlenk reactor and subjected to freeze-vacuum-thaw cycles three times using liquid N_2. After the so-called impregnation process, the mixture was washed with copious anhydrous ethanol, and then re-dispersed in 50 mL anhydrous ethanol. Subsequently, 3-aminopropyltriethoxysilane (APS, 1 mL, 50% in anhydrous ethanol) was added into the suspension and stirred for another 8 h forming hydrogen bond with PCL to further block the pores. The resultant solid was filtered, washed with tetrahydrofuran and ethanol, and then dried under vacuum. To ensure that the PCL and APS physically adsorbed on MSN was removed completely, the washing procedure was repeated until the weight loss of PCL-MSN (calculated by TGA) did not change. The graft ratio of PCL was about 17 wt% evaluated by TGA. The as-synthesized PCL-MSN (30 mg) was dispersed in 10 mL of DMF, and then 10 mg of PAA (M_w = 2500 Da) was dissolved into the mixture. The mixture was stirred at room temperature for 24 h to form hydrogen bond between PAA and the amino group at the surface of PCL-MSN. After the reaction, the mixture was centrifuged and washed with copious ethanol. A similar process to that described above for the PCL-MSN particles to remove any physical absorbed was again performed. The final graft ratio of PAA was about 17 wt %. The amount of loaded drug for MSN was determined by emission peak at 560 nm in fluorescence spectra.

Stimulated Drug Release: In the pH and esterase triggered drug release experiment, a certain amount of Rhodamine 6G loaded PAA-PCL-MSNs powder was dispersed in 50 mL of 4 different type of PBS buffer (i: pH 5.5 in the presence of 4 mg/L esterase, ii: pH 5.5 in the absence of 4 mg/L esterase, iii: pH 7.4 in the presence of 4 mg/L esterase and iv: pH 7.4 in the absence of 4 mg/L esterase) at 25 °C. Subsequently, 2 mL of supernatant was taken periodically from the suspension at 25 °C followed by centrifugation (15 000 rpm, 20 min). The release of Rhodamine 6G from the pores to the buffer solution was determined by fluorescence emission spectroscopy (em at 560 nm).

Endocytosis and In Vitro Release of Drug Loaded PAA-PCL-MSN: HeLa cells were seeded in growth medium for 24 h prior to the experiment. After 24 h, selected cells are cultured in glass bottom Petri dish with growth medium containing 10% fetal bovine serum (FBS), 1% antibiotics and 0.1 mg drug loaded PAA-PCL-MSNs for different hours, then are washed with PBS for 3 times and fixed by 4% paraformaldehyde solution. After 30 min fixation, the cells are washed by PBS and subjected to fluorescent imaging. For confocal imaging of MSN-Rhodamine 6G and MSN-DOX uptake, SK-N-BE(2) and MRC-5 cells (5000 cells/dish) were plated in 35 mm cultured dishes which were pre-coated with poly-D-lysine hydrobromide for 10 min and left to grow for 3 days. Two types of confocal microscopes—Zeiss LSM 780 and Leica TCS SP5—were utilized to acquire images, both equipped with an environmental chamber which controls the atmospheric conditions, humidity and temperature for live-cell imaging. FLIM measurements were acquired using a Picoquant Microtime200 inverted confocal microscope with a 63X 1.2NA water-immersion objective. DOX was excited using 550 nm diode laser at a repetition rate of 40 MHz. Fluorescence emission was detected 550 nm long-pass filter using a single-photon avalanche diode (SPAD) and PicoHarp300 TCSPC electronics. Fluorescein was used to calibrate the phasor plot to a monoexponential lifetime of 4 ns. Phasor analysis was performed using simFCS (developed by Enrico Gratton, Laboratory of Fluorescence Dynamics, Irvine, CA).

In Vitro Cytotoxicity (MTT Method): Cytotoxicity experiments were performed using HeLa cells. Before experiments, cells were cultured in 10 mL growth medium containing 10% fetal bovine serum (FBS), 1% antibiotics. Cytotoxicity assay were performed in 96-wells microtiter plates with seeding density, 10 000 cells per well. Microtiter plates containing cells were pre-incubated for 24 h at 37 °C in order to allow stabilization before the addition of the test substance (MSNs, PAA, PCL and PAA-PCL-MSNs). The plates were incubated with the test substance for 24 h and 48 h respectively at 37 °C and 5% CO_2. Then 5 µL MTT solution (5 mg/mL in PBS) was added to each well to evaluate cell viability. After 2 h at 37 °C, the solution was removed. 100 uL DMSO was added to dissolve cells. After 30 min incubation under 37 °C, the viability was measured through microreader.

Cell Viability: The cytotoxicity of free DOX or DOX loaded PAA-PCL-MSNs were tested in neuroblastoma cells (SK-N-BE (2)) and human fetal lung fibroblast cells (MRC-5) *via* the Alamar Blue cellular metabolic activity (cell proliferation) assay. The cells were seeded at 5,000 cells/well for MRC5 and 1250 cells/well for SK-N-BE(2)/TGL in 96 well tissue culture plates and incubated for 24 h. The medium was then replaced with fresh medium containing free DOX or DOX loaded PAA-PCL-MSNs.

At 72 h post drug/particle incubation, treatments were removed and fresh media was added (100 µL) followed by the addition of the resazurin solution (20 µL) to each well and the cells were incubated for 6 h and absorbance measured using a Benchmark Plus microplate spectrophotometer reader (Biorad) at 570 nm (595 nm reference wavelength). Cell viability was determined as a percentage of untreated control cells, and IC_{50} values were calculated via regression analysis using Graphpad Prism 5. Experiments were repeated three times by quadruplicate.

Characterization: Transmission electron microscopy (TEM) images were recorded on a Philips CM200 transmission electron microscope operated at 200 kV. For the TEM observation, samples were obtained by dropping 5 µL of solution onto carbon-coated copper grids. All the TEM images were visualized without staining. The surface areas were measured using the Brunauer Emmett Teller (BET) method, and the pore size distributions were calculated by the Barrett Joyner Halenda (BJH) method. The infrared (IR) spectra were measured by AVATAR 320 FT-IR using KBr pellets. The fluorescence spectra were recorded using a Varian Cary Eclipse spectrometer. MS spectrum were recorded using LTQ-Orbitrap (Thermo Scientific, San Jose, CA) operating at ion trap mass spectrometry (ITMS) with *m/z* range 150–2000 Da. The ultraviolet-visible (UV–vis) spectra were measured with dilute aqueous solution in a 2 mm thick quartz cell using a SHIMADZU UV-2401 PC spectrophotometer. All pH value measurements were carried out on a Sartorius BECKMAN F 34 pH meter. The zeta potentials were measured by a Malvern Zetasizer Nano Series running DTS software and using 4 mW He-Ne laser operating at a wavelength of 633 nm and avalanche photodiode (APD) detector. Thermogravimetric analysis was measured by PerkinElmer STA 6000 simultaneous thermal analyzer from 25 °C to 800 °C at heating rate of 10 °C/min. Intracellular release was monitored by fluorescence spectroscopy and confocal fluorescence microscopy using a NIKON ECLIPSE 600 microscope equipped with a fluorescent NIKON Y-FL lamp; ex = 530 nm, em = 570 nm for Rhodamine 6G, ex = 480 nm, em = 560 nm for DOX.

Supporting Information

Supporting Information is available from the Wiley Online Library or from the author.

Acknowledgements

The authors thank the Australian Research Council (DP110902183) and the National Health and Medical Research Council (APP1024723) and the University of New South Wales for financial support for various aspects of this research work. The author would also like to thanks Dr. Jason Scott for the BET measurements.

Received: July 15, 2014
Published online: September 5, 2014

[1] R. Duncan, *Nat. Rev. Cancer* **2006**, *6*, 688.
[2] a) S. Biswas, K. Kinbara, T. Niwa, H. Taguchi, N. Ishii, S. Watanabe, K. Miyata, K. Kataoka, T. Aida, *Nat. Chem.* **2013**, *5*, 613; b) D. Peer, J. M. Karp, S. Hong, O. C. Farokhzad, R. Margalit, R. Langer, *Nat. Nanotechnol.* **2007**, *2*, 751; c) G. Von Maltzahn, J. H. Park, K. Y. Lin, N. Singh, C. Schwöppe, R. Mesters, W. E. Berdel, E. Ruoslahti, M. J. Sailor, S. N. Bhatia, *Nat. Mater.* **2011**, *10*, 545.
[3] a) D. Schmaljohann, *Adv. Drug Delivery Rev.* **2006**, *58*, 1655; b) L. Yuan, Q. Q. Tang, D. Yang, J. Z. Zhang, F. Y. Zhang, J. H. Hu, *J. Phys. Chem. C* **2011**, *115*, 9926.
[4] C. d. l. H. Alarcon, S. Pennadam, C. Alexander, *Chem. Soc. Rev.* **2005**, *34*, 276.
[5] J. Chen, X. Z. Qiu, J. Ouyang, J. M. Kong, W. Zhong, M. M. Q. Xing, *Biomacromolecules* **2011**, *12*, 3601.
[6] M. Zelzer, S. J. Todd, A. R. Hirst, T. O. McDonald, R. V. Ulijn, *Biomater. Sci.* **2013**, *1*, 11.
[7] S. Mura, J. Nicolas, P. Couvreur, *Nat. Mater.* **2013**, *12*, 991.
[8] a) K. Engin, D. B. Leeper, J. R. Cater, A. J. Thistlethwaite, L. Tupchong, J. D. Mcfarlane, *Int. J. Hyperthermia* **1995**, *11*, 211; b) V. P. Torchilin, *Nat. Rev. Drug Discovery* **2005**, *4*, 145.
[9] L. E. Gerweck, K. Seetharaman, *Cancer Res.* **1996**, *56*, 1194.
[10] M. A. Dobrovolskaia, S. E. McNeil, *Nat. Nanotechnol.* **2007**, *2*, 469.
[11] T. M. Allen, P. R. Cullis, *Science* **2004**, *303*, 1818.
[12] a) D. Xiao, H.-Z. Jia, J. Zhang, C.-W. Liu, R.-X. Zhuo, X.-Z. Zhang, *Small* **2014**, *10*, 591; b) Z. Li, J. C. Barnes, A. Bosoy, J. F. Stoddart, J. I. Zink, *Chem. Soc. Rev.* **2012**, *41*, 2590; c) I. I. Slowing, B. G. Trewyn, S. Giri, V. S. Y. Lin, *Adv. Funct. Mater.* **2007**, *17*, 1225; d) B. G. Trewyn, S. Giri, I. I. Slowing, V. S. Y. Lin, *Chem. Commun.* **2007**, 3236; e) B. G. Trewyn, I. I. Slowing, S. Giri, H. T. Chen, V. S. Y. Lin, *Acc. Chem. Res.* **2007**, *40*, 846.
[13] S. Angelos, N. M. Khashab, Y. W. Yang, A. Trabolsi, H. A. Khatib, J. F. Stoddart, J. I. Zink, *J. Am. Chem. Soc.* **2009**, *131*, 12912.
[14] E. Aznar, R. Casasús, B. García-Acosta, M. D. Marcos, R. Martínez-Máñez, F. Sancenón, J. Soto, P. Amorós, *Adv. Mater.* **2007**, *19*, 2228.
[15] S. Giri, B. G. Trewyn, M. P. Stellmaker, V. S. Y. Lin, *Angew. Chem. Int. Ed.* **2005**, *44*, 5038.
[16] B. Chang, D. Chen, Y. Wang, Y. Chen, Y. Jiao, X. Sha, W. Yang, *Chem. Mater.* **2013**, *25*, 574.
[17] a) A. Agostini, L. Mondragón, L. Pascual, E. Aznar, C. Coll, R. Martínez-Máñez, F. Sancenón, J. Soto, M. D. Marcos, P. Amorós, A. M. Costero, M. Parra, S. Gil, *Langmuir* **2012**, *28*, 14766; b) N. Singh, A. Karambelkar, L. Gu, K. Lin, J. S. Miller, C. S. Chen, M. J. Sailor, S. N. Bhatia, *J. Am. Chem. Soc.* **2011**, *133*, 19582.
[18] H. Yan, C. Teh, S. Sreejith, L. Zhu, A. Kwok, W. Fang, X. Ma, K. T. Nguyen, V. Korzh, Y. Zhao, *Angew. Chem. Int. Ed.* **2012**, *51*, 8373.
[19] X. Ma, O. S. Ong, Y. Zhao, *Biomater. Sci.* **2013**, *1*, 912.
[20] B. Chang, X. Sha, J. Guo, Y. Jiao, C. Wang, W. Yang, *J. Mater. Chem.* **2011**, *21*, 9239.
[21] X. Chen, X. Cheng, A. H. Soeriyadi, S. M. Sagnella, X. Lu, J. A. Scott, S. B. Lowe, M. Kavallaris, J. J. Gooding, *Biomater. Sci.* **2014**.
[22] S. Angelos, Y.-W. Yang, N. M. Khashab, J. F. Stoddart, J. I. Zink, *J. Am. Chem. Soc.* **2009**, *131*, 11344.
[23] Y. Amir, E. Ben-Ishay, D. Levner, S. Ittah, A. Abu-Horowitz, I. Bachelet, *Nat Nano* **2014**, *9*, 353.
[24] H. Peng, R. Dong, S. Wang, Z. Zhang, M. Luo, C. Bai, Q. Zhao, J. Li, L. Chen, H. Xiong, *Int. J. Pharm.* **2013**, *446*, 153.
[25] M. A. Woodruff, D. W. Hutmacher, *Prog. Polym. Sci.* **2010**, *35*, 1217.
[26] K. Ulbrich, V. Šubr, *Adv. Drug Delivery Rev.* **2004**, *56*, 1023.
[27] M.-H. Kim, H.-K. Na, Y.-K. Kim, S.-R. Ryoo, H. S. Cho, K. E. Lee, H. Jeon, R. Ryoo, D.-H. Min, *ACS Nano* **2011**, *5*, 3568.
[28] D. Goren, A. T. Horowitz, D. Tzemach, M. Tarshish, S. Zalipsky, A. Gabizon, *Clinical Cancer Res.* **2000**, *6*, 1949.
[29] L. M. Pan, Q. J. He, J. N. Liu, Y. Chen, M. Ma, L. L. Zhang, J. L. Shi, *J. Am. Chem. Soc.* **2012**, *134*, 5722.
[30] S. M. Sagnella, H. Duong, A. MacMillan, C. Boyer, R. Whan, J. A. McCarroll, T. P. Davis, M. Kavallaris, *Biomacromolecules* **2013**, *15*, 262.
[31] X. W. Dai, Z. L. Yue, M. E. Eccleston, J. Swartling, N. K. H. Slater, C. F. Kaminski, *Nanomed. Nanotechnol.* **2008**, *4*, 49.
[32] J. S. Basuki, H. T. T. Duong, A. Macmillan, R. B. Erlich, L. Esser, M. C. Akerfeldt, R. M. Whan, M. Kavallaris, C. Boyer, T. P. Davis, *ACS Nano* **2013**, *7*, 10175.
[33] S. P. Hudson, R. F. Padera, R. Langer, D. S. Kohane, *Biomaterials* **2008**, *29*, 4045.
[34] M. Vallet-Regi, A. Ramila, R. P. del Real, J. Perez-Pariente, *Chem. Mater.* **2001**, *13*, 308.